Anisotropic plasticity of nanocrystalline Ti: A molecular dynamics simulation*

Minrong An(安敏荣)[1], Mengjia Su(宿梦嘉)[2], Qiong Deng(邓琼)[2,†], Haiyang Song(宋海洋)[1,‡], Chen Wang(王晨)[1], and Yu Shang(尚玉)[1]

[1] College of Materials Science and Engineering, Xi'an Shiyou University, Xi'an 710065, China
[2] Fundamental Science on Aircraft Structural Mechanics and Strength Laboratory, Northwestern Polytechnical University, Xi'an 710072, China

(Received 11 December 2019; revised manuscript received 22 January 2020; accepted manuscript online 30 January 2020)

Using molecular dynamics simulations, the plastic deformation behavior of nanocrytalline Ti has been investigated under tension and compression normal to the $\{0001\}$, $\{\bar{1}010\}$, and $\{\bar{1}2\bar{1}0\}$ planes. The results indicate that the plastic deformation strongly depends on crystal orientation and loading directions. Under tension normal to basal plane, the deformation mechanism is mainly the grain reorientation and the subsequent deformation twinning. Under compression, the transformation of hexagonal-close packed (HCP)-Ti to face-centered cubic (FCC)-Ti dominates the deformation. When loading is normal to the prismatic planes (both $\{\bar{1}010\}$ and $\{\bar{1}2\bar{1}0\}$), the deformation mechanism is primarily the phase transformation among HCP, body-centered cubic (BCC), and FCC structures, regardless of loading mode. The orientation relations (OR) of $\{0001\}_{\rm HCP}||\{111\}_{\rm FCC}$ and $\langle\bar{1}210\rangle_{\rm HCP}||\langle110\rangle_{\rm FCC}$, and $\{10\bar{1}0\}_{\rm HCP}||\{1\bar{1}0\}_{\rm FCC}$ and $\langle0001\rangle_{\rm HCP}||\langle010\rangle_{\rm FCC}$ between the HCP and FCC phases have been observed in the present work. For the transformation of HCP $\rightarrow$ BCC $\rightarrow$ HCP, the OR is $\{0001\}_{\alpha1}||\{110\}_{\beta}||\{10\bar{1}0\}_{\alpha2}$ (HCP phase before the critical strain is defined as α_1-Ti, BCC phase is defined as β-Ti, and the HCP phase after the critical strain is defined as α_2-Ti). Energy evolution during the various loading processes further shows the plastic anisotropy of nanocrystalline Ti is determined by the stacking order of the atoms. The results in the present work will promote the in-depth study of the plastic deformation mechanism of HCP materials.

Keywords: molecular dynamics simulation, nanocrystalline Ti, anisotropic plasticity, deformation mechanism

PACS: 62.25.–g, 61.46.–w, 64.70.Nd, 02.70.Ns **DOI:** 10.1088/1674-1056/ab7188

1. Introduction

Titanium (Ti) has been regarded as strategically important metal due to its excellent properties within a very wide temperature window, and exceptionally strong resistance to acid and alkali attack. Ti and its alloys have a number of outstanding qualifications such as low density, high specific strength, decent ductility, and good biocompatibility.[1–4] As such, they are widely used in rockets and other aerospace applications, which earn it the nickname of "space metal".[5,6] Single phase Ti may be characterized as the hexagonal close-packed (HCP) structure, namely stable α phase at room temperature, while undergoing an allotropic phase transition to the body-centered cubic (BCC) phase at high temperature (882 ℃).[1] Different from the ample slip systems in face-centered cubic (FCC) and BCC structured metal, the slip system in HCP metal is finite. However, there are profuse twinning systems in HCP metal. Therefore, HCP metals usually undergo plastic deformation through twinning deformation rather than dislocation slip. It has been reported that there are six types of twins in deformed Ti,[7,8] including tensile twins of $\{11\bar{2}1\}\langle11\bar{2}6\rangle$, $\{10\bar{1}2\}\langle10\bar{1}1\rangle$, and $\{11\bar{2}3\}\langle33\bar{6}2\rangle$, as well as compressive twins of $\{10\bar{1}1\}\langle10\bar{1}2\rangle$, $\{11\bar{2}2\}\langle11\bar{2}3\rangle$, and $\{11\bar{2}4\}\langle22\bar{4}3\rangle$. Moreover, the "twin-like" reorientation[9–12] has also been investigated as a new deformation mechanism for HCP metals. That is to say, although dislocation propagation is limited, HCP metals can undergo plastic deformation in other forms to ensure good plasticity.

It is known that plastic properties are dependent on crystal orientation for crystalline materials, which also determines the plastic deformation mechanism of the materials. Due to the lower spatial symmetry than BCC and FCC structures, HCP metals and alloys dramatically show anisotropic plasticity with loading applied along different crystal orientations. There have been numerous researches on the effect of crystal orientation on plastic deformation of HCP materials, and have obtained fruitful theoretical results in recent years. Researches on the plastic behaviors of HCP metallic materials are mainly focused on several common materials such as Mg,[13,14] Ti,[15–21] and Zr.[22] Ni *et al.*[13] simulated the tensile properties of HCP-Mg nanowire in $\langle11\bar{2}0\rangle$ orientation and discovered primary and sequential secondary twinning dominated the plastic behavior, which finally resulted in ultrahigh 60% elongation. Chen *et al.*[14] performed molecular dynam-

*Project supported by the National Natural Science Foundation of China (Grant No. 11572259), the Natural Science Foundation of Shaanxi Province, China (Grant Nos. 2019JQ-827, 2018JM1013, and 2018JQ5108), and the Scientific Research Program Funded by Shaanxi Provincial Education Department, China (Grant No. 19JK0672).

†Corresponding author. E-mail: dengqiong24@nwpu.edu.cn
‡Corresponding author. E-mail: gsfshy@sohu.com

ics (MD) simulations exploring basal/prismatic twin boundary migration with compression loading applied along $[10\bar{1}0]$ of parent phase. And an abnormal reversible HCP $\rightarrow$ FCC phase transformation was observed, which was induced by the misfit strain between the matrix and twin. The fact indicates that pure Mg can also achieve plastic deformations through phase transformation under certain crystal structure and loading mode, although its main plastic deformation is twinning deformation. As for the HCP-Ti, ample efforts have been made to approach the nature of plastic deformation mechanism. For the case of tension loading applied along c axis, Ren *et al.*[15] reported that the $\{10\bar{1}2\}\langle 10\bar{1}1\rangle$ twin is observed when tension loading is applied along [0001] direction, and the phase transformation from HCP to FCC has also been another new deformation mechanism during the tension process. An *et al.*[16] further found that the formation of basal/prismatic interface and the motion of SFs in "twin" grains dominate the deformation mechanism in [0001] tension. As for the compression loading applied along c axis, both plastic behaviors in simulations and experiments exhibit different deformation patterns compared to the condition of tension loading. Yu and his colleagues[17] performed *in situ* TEM experiments for the compression testing on single crystal Ti oriented along c axis, they found that $\langle c+a\rangle$ dislocations are the preferred slip mode and $\langle c+a\rangle$ dislocations could operate as single-arm sources. In simulation, Ren and his coworkers further confirmed the deformation mechanism in all [0001]-oriented nanopillars is dominated by the pyramidal $\langle c+a\rangle$ slip.[18] While An *et al.*[16] found something new during the compression loading imposed along [0001] direction of Ti nanoplate with internal stacking faults (SFs). And FCC band emerges during the compression and the blockage of SF boundary to the FCC-Ti phase boundary in compression is the main deformation mechanism in this condition. In the case of loading applied for the prismatic plane of the HCP-Ti, the results are also different from the previous conclusions. Yu[19] tested the tensile properties of Ti nanopillar along $[2\bar{1}\bar{1}0]$ direction through *ex-situ* and *in situ* experiments. They concluded that the SFs are possible to be activated, and the presence of SFs has consequences on the work hardening and plastic flow: the SFs debris interact with prismatic dislocations, and serve as obstacle to hinder runaway dislocation avalanche. Ren *et al.*[18] presented the simulation results that the plasticity of the $[11\bar{2}0]$-oriented nanopillars with compressive strain is predominantly produced by the edge dislocation lines. Moreover, Chen[20] reported very interesting transitory phase transformation between BCC, HCP, and FCC structures in HCP-Ti when compression loading is applied along the $[10\bar{1}0]$ axis.

According to the above fruitful results, one thing should be emphasized is that both crystal orientations and loading directions have a dramatic influence on the plastic deformation behavior of HCP materials, and Ti shows anisotropic plasticity under various working conditions. However, the previous results are too scattered and lack of systematic research on the influence of crystal orientations and loading directions on the plastic behavior of HCP materials. Moreover, due to the large difference between the models adopted in simulations and experiments, the impact of the model size on the mechanical behaviors of nanometer materials is unknown. Despite the ample literature work, it is still unclear how the coupled crystal orientations and loading directions affects the microstructure evolution of HCP-Ti, whether there is plastic anisotropy during loading process. In this work, the effect of crystal orientations and loading conditions on the deformation behaviors of HCP-Ti is investigated using MD simulations, which has been used widely to explain the mechanical behavior and detailed deformation process of materials.[23–28] The results show that the deformation behavior strongly depends on orientation and loading mode. This work will provide a new sight in the orientation-dominated plastic deformation mechanism.

2. Simulation methods

In our previous work, we have investigated the effect of SF on the mechanical properties of nanocrystal Ti. For comparison, similar models are constructed in this work. And the details of the initial models are presented in Fig. 1. For HCP structure, the close-packed plane is (0001) plane, and the stacking sequence of atomic planes is ABABAB$\cdots$, as shown in Figs. 1(b)–1(d). The crystal orientations of the basal plane model are X-$[\bar{1}2\bar{1}0]$, Y-[0001], and Z-$[\bar{1}010]$; and the orientations of the prismatic plane I model are X-$[\bar{1}2\bar{1}0]$, Y-$[\bar{1}010]$, and Z-[0001]; while the orientations for the prismatic plane II are X-$[\bar{1}010]$, Y-$[\bar{1}2\bar{1}0]$, and Z-[0001]. The lattice constants for α-Ti at room temperature are $a = 0.295$ nm, $c = 0.468$ nm, and $c/a = 1.578$, respectively. In the present work, the dimensions of the samples in X and Z directions are 3.0 nm and 10.3 nm, and the dimension in Y direction is 45.0 nm. Periodic boundary conditions are applied in X and Y directions, while Z direction is a free boundary condition.

The accuracy of the potential directly affects the reliability of the simulation results. The potential used for describing the interaction of metal atoms has evolved from embedded-atom method potential (EAM) to the second-nearest-neighbor (2NN) modified EAM.[29–31] The 2NN MEAM is an improved one of describing surface relaxation, thermal expansion, and amorphous structure based on the previously developed Baskes MEAM Si potential. It can describe various fundamental physical properties: elastic, structural, point defect, surface, thermal (except melting point), and cluster. However, the EAM potential used in this work is developed by Wadley and Zhou,[32,33] which has been verified to describe the Ti–Ti interatomic interactions correctly.[34–36] It is well fitted to

basic material properties such as lattice constants, elastic constants, bulk moduli, vacancy formation energies, and sublimation energies. Verlet integration algorithm is used to obtain the motion of Newton atoms with a time step of 3 fs. To obtain the energy minimum state before loading, the structure is initially equilibrated for 24 ps in NVT ensemble, and 30 ps in NPT ensemble. Upon the completion of equilibrium process, tension or compression loading is applied perpendicularly to the basal or prismatic planes for all the models with the strain rate of 6.7×10^8 s^{-1}. And the temperature is fixed as 10 K during the simulation process. For discerning the different crystal structure, and lattice defects, the common neighbor analysis (CNA)[37] is applied by using the Open Visualization Tool (OVITO).[38] The dislocation extraction algorithm (DXA) is used to identify dislocations in the simulations. It can converts identified dislocation networks into continuous lines and determines their Burgers vectors in a fully automated fashion even in highly distorted crystal regions, which is a general and powerful method for characterizing the topological structure of dislocations from atomic simulations.[39,40] In this work, the HCP, BCC, FCC, and non-structure atoms are colored red, blue, green, and white gray, respectively.

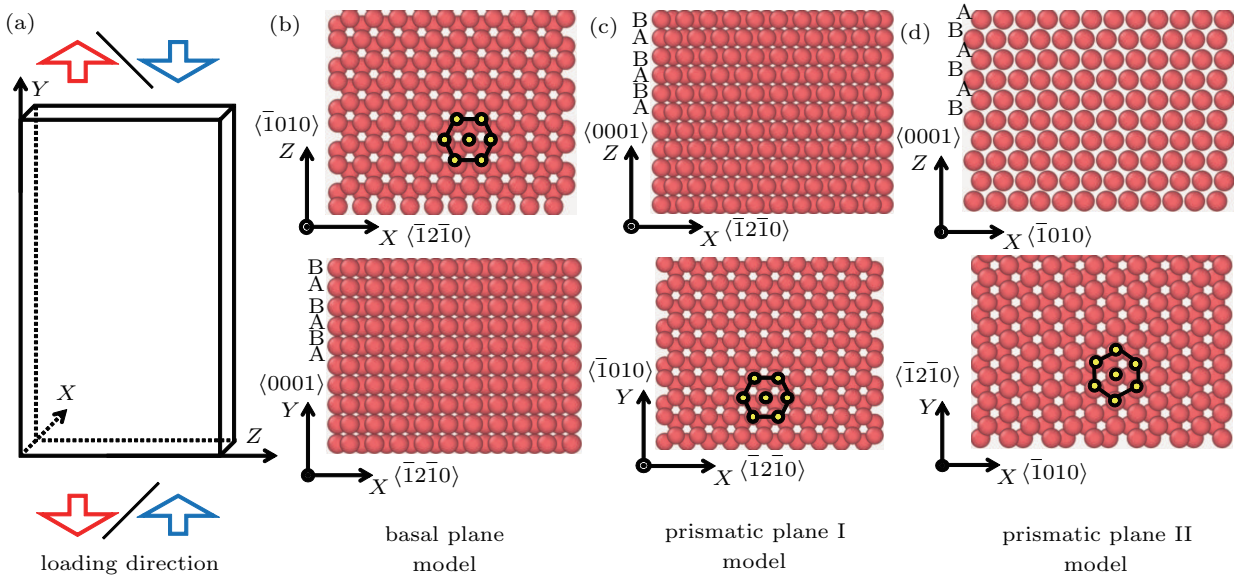

Fig. 1. (a) The schematic diagram of the nanocrystal HCP-Ti under tension/compression loadings. (b)–(d) The details of the initial models of (b) basal plane model; (c) prismatic plane I model; (d) prismatic plane II model. In the simulation, the tension/compression loading is applied perpendicular to basal plane and prismatic planes.

3. Results

3.1. Plastic deformation of Ti under loading perpendicular to basal plane

3.1.1. Tension loading

The deformation behavior of nanocrystal Ti under tension loading perpendicular to basal plane is investigated, and the atomic configurations evolution is demonstrated in Fig. 2. It is observed from Fig. 2(a) that some new grains nucleate from the free surfaces at the strain of 7.6%. And the inset of Fig. 2(a) shows the atomic stacking sequence of the initial Y–Z plane. The corresponding DXA in Fig. 2(b) shows that the dislocation networks generate between the new grains and the matrix. $1/3\langle\bar{1}100\rangle$ partial dislocations in basal slip system and $1/9\langle\bar{1}103\rangle$ partial dislocations in the prismatic slip system are observed during the tension process. The new grains expand continuously with the increase of strain until they encounter each other or reach the free surfaces of the model. Actually, the crystal orientation in tensile direction of the new grain is different from the parent Ti laminate, and there are three twin variants inside newly formed structure, as displayed in Fig. 2(c). The inset picture shows the Y–Z plane's atomic stacking sequence of twin variant I during the tension process. Comparing with the inset picture of Fig. 2(a), the stacking sequence of the matrix and variant is quite disparate, and the grain reorientation dominates the initial plastic deformation of the material. With the tensile strain going on, a second linear elastic stage is observed due to the formation of the new grains. After the elastic stage, some defects first emerge at the junction of new grain boundaries and free surface. Since then, some new grains nucleate from the free surfaces and grow in the Ti laminate, and a polycrystalline model is obtained at the strain of 16.8%, as shown in Figs. 2(d)–2(e). For the larger tensile strain, twinning and slip bands emit from the grain boundaries or free surfaces and propagate at the internal grains, as plotted in Fig. 2(f).

For exploring the details of the grain reorientation in Fig. 2(a), the close-up section of the reorientation is presented in Fig. 3(a). It is observed from Fig. 3(a) that the orientation of the new grain is about 90° rotated from the matrix lattice, which can be regarded as the "twin" phase. That is

to say, the basal plane in the parent body transforms into the prismatic planes of the new lattice. Microstructure indicates that the basal/prismatic (B/P) interface is formed between the two phases. Due to the misorientation, the B/P interface is a semi-coherent interface, and there are mismatched dislocations at the interface, as shown in Fig. 2(b). The phenomenon in this work is consistent with Ren's observation in HCP-Ti nanopillars,[15] and the detailed structure is shown in Fig. 3(b). The plateau and stepped region on the B/P interface emerge between the matrix and the "twin" phase. One thing should be noted here is that angle between the matrix and the twin phase in $\{10\bar{1}2\}$ twins is 84.7° in HCP-Ti. However, the angle between the two phases is about 90° in the present work, which is a little larger than the angle of $\{10\bar{1}2\}$ twins.

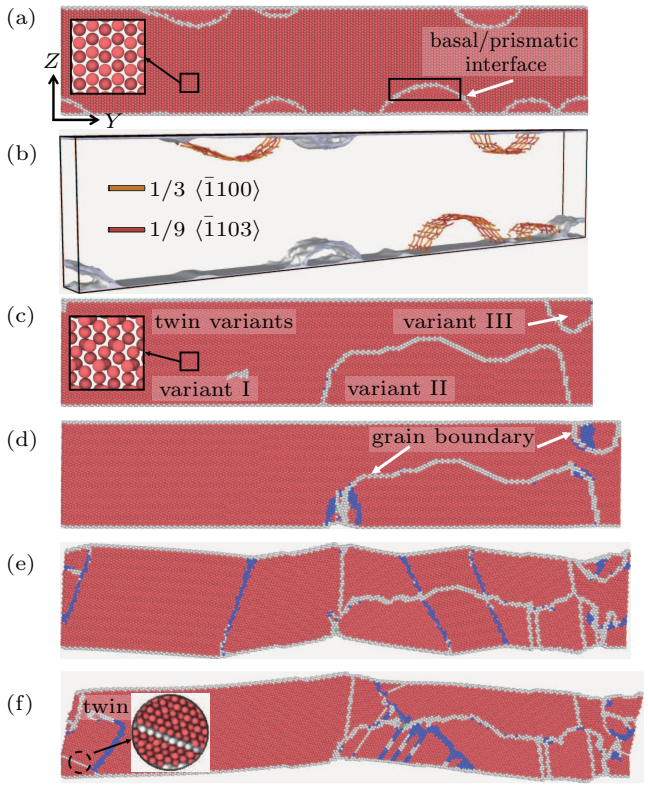

Fig. 2. The atomic configurations of the nanocrystal Ti at different strains when the tensile loading is perpendicular to basal plane at 10 K for (a) $\varepsilon = 7.6\%$, (b) $\varepsilon = 7.6\%$, (c) $\varepsilon = 8.4\%$, (d) $\varepsilon = 14.1\%$, (e) $\varepsilon = 16.8\%$, and (f) $\varepsilon = 25.1\%$.

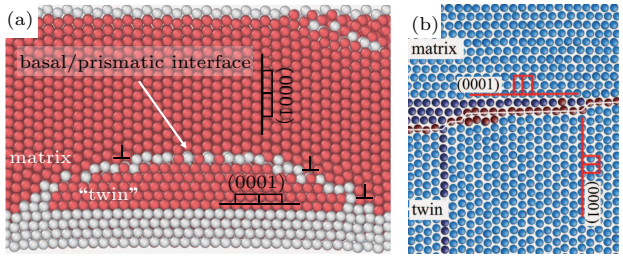

Fig. 3. (a) The close-up section of the reorientation shown in Fig. 2(a). (b) The details of "twin" shown in tension of Ti reported by Ren.[15]

Therefore, we suppose that the formation of the B/P interface during the tension process along *c* axis is a twin-like behavior. The conclusions are also consistent with the prismatic/basal interface reported in HCP-Mg[9,10] and the serrated basal/prismatic interface in HCP-Co.[11] In the results of HCP-Mg, Liu *et al.*[9] considered that reorientation is twin-like structure. As the strain concentration occurring near the interface or other defects, the basal plane of the matrix lattice is no longer completely parallel to the prismatic plane of the new lattice in many regions, and the orientation of the crystals between these interfaces is close to 90°, rather than 86.3° of $\{10\bar{1}2\}$ twins. While for the HCP-Co, Wang *et al.*[11] thought that both the coherent twins and the basal/prismatic interfaces exist at the serrated interface between the new grain and the matrix. Therefore, the formation of B/P interface is an effective complement to the plastic behavior of HCP metal.

3.1.2. Compression loading

As the compression loading applied normal to basal plane, the deformation behavior of nanocrystal Ti is greatly different from the tension condition, and figure 4 shows the atomic configurations of the nanocrystal Ti at various compressive strains. It is observed from Fig. 4(a) that the FCC-Ti nucleates from the free surfaces at the strain of 4.1%. As the compression loading continues, the FCC-Ti region expands and the interphase interface forms between the two phases. The illustration of Fig. 4(b) shows a partial enlargement between the HCP and FCC phases, and there are dislocations at the interfaces. DXA further shows that dislocations form

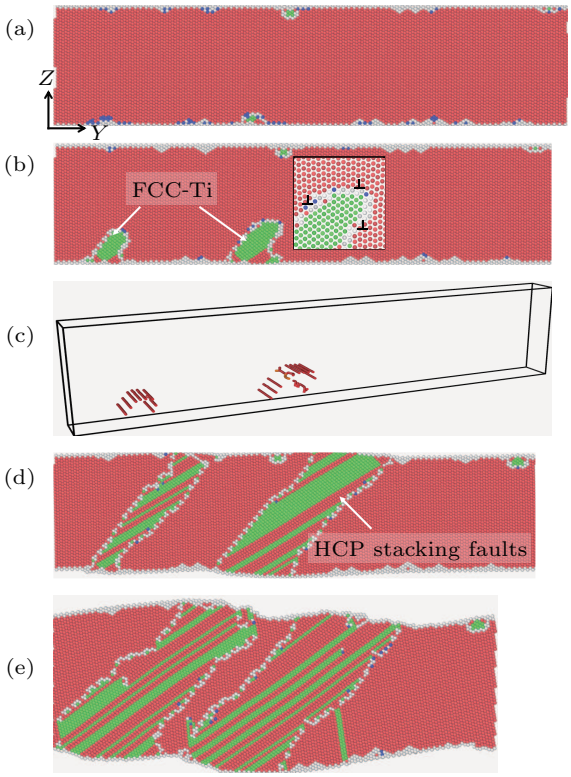

Fig. 4. The atomic configurations of the nanocrystal Ti at different strains when the compression loading is normal to basal plane at 10 K for (a) $\varepsilon = 4.1\%$, (b) $\varepsilon = 4.6\%$, (c) $\varepsilon = 4.6\%$, (d) $\varepsilon = 5.9\%$, and (e) $\varepsilon = 19.1\%$.

in the interface due to different crystal structures (Fig. 4(c)). With the increase of compressive strain, FCC-Ti grows constantly until the interfaces reach the opposite free surfaces. Meanwhile, HCP SFs emerge in the FCC grains as the result of partial dislocations propagation, as shown in Figs. 4(d) and 4(e). And the dislocations propagation and the accumulation of SFs in FCC-Ti dominate the subsequent plastic deformation.

3.2. Plastic deformation of Ti under loading vertical to prismatic plane I

3.2.1. Tension loading

As the tension loading applied perpendicularly to the prismatic plane I, the plastic behavior is different from the tensile behavior of Ti under loading normal to basal plane, exhibiting obvious plastic anisotropy.

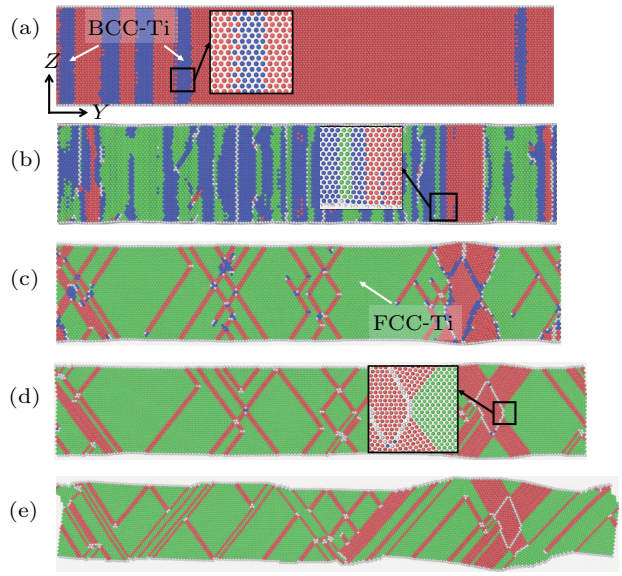

Fig. 5. The atomic configurations of the nanocrystal Ti at different strains when the tension loading is perpendicular to prismatic plane I at 10 K for (a) $\varepsilon = 10.7\%$, (b) $\varepsilon = 10.9\%$, (c) $\varepsilon = 11.2\%$, (d) $\varepsilon = 17.9\%$, and (e) $\varepsilon = 30.1\%$.

Figure 5 depicts the microstructure evolution of nanocrystal Ti in Y–Z plane during the stretch process. As shown in Fig. 5(a), some BCC-Ti atoms occur at the strain of 10.7%, the inset indicates that partial atoms in $\{0001\}$ basal plane of parent phase move along the $\langle 10\bar{1}0\rangle$ direction and finally form the BCC structure. And no dislocation motions are found during the phase transformation. Subsequently, the BCC-Ti regions continue to expand and FCC-Ti phases appear on both sides of the model, described in Fig. 5(b). The inset describes the orientation relationship between the HCP, BCC, and FCC lattices, which is $\{10\bar{1}0\}_{\mathrm{HCP}} || \{110\}_{\mathrm{BCC}} || \{1\bar{1}0\}_{\mathrm{FCC}}$ for different structures. With the increase of tension strain, the FCC-Ti phase regions expand continuously accompanied by the formation of HCP SFs induced by propagation of partial dislocations at the internal grain. Simultaneously, the BCC atoms gradually vanish with the increase of tensile strain. Since then, the interaction between the partial dislocations and SFs dominates the plastic behavior, as shown in Figs. 5(c)–5(e). During the process, the BCC structure seems to provide a bridge for the phase transformation of HCP to FCC crystal, and the transient BCC phase transformation in nanocrystal Ti allows the transition between different crystalline structures without dislocation motion.

3.2.2. Compression loading

Figure 6 shows the atomic configurations of the nanocrystal Ti at different strains when the compression loading is normal to prismatic plane I. It is observed that some BCC-Ti atoms emerge at the strain of 7.4%, as shown in Fig. 6(a). The illustration exhibits the crystalline relationship between the HCP and BCC structures, and the atomic shuffles also contributes to the formation of BCC crystal. When the compression strain increases to 9.8%, the HCP-Ti has transformed to BCC-Ti completely. Different from the phenomenon of tension, the BCC phase transition in compression is relatively stable. As the strain increases to 11.7%, the BCC crystal begins to transform to HCP structure, and there are some interfaces between HCP-Ti and BCC-Ti regions in the crystal, as shown in Fig. 6(c). What should be noted here is that the newly formed HCP-Ti is different from the crystal orientation of the initial HCP phase, which has been rotated at a certain angle in space relative to the parent phase, as shown in the inset of Fig. 6(c). The BCC-Ti has transformed to HCP-Ti again at the strain of 15.1%. The interesting thing is that there are many grain boundaries in the nanocrystal Ti, *i.e.*, the sample changes from single crystal to polycrystalline structure, displayed in Fig. 6(d). Simultaneously, some SFs occur at the internal grains resulting from the movement of partial dislocations. Upon further loading, dense FCC SFs in HCP-Ti accumulate and form SFs band, namely the FCC-Ti phase. Hereafter, numerous HCP SFs form and interact with the grain boundary, as shown in Figs. 6(e) and 6(f).

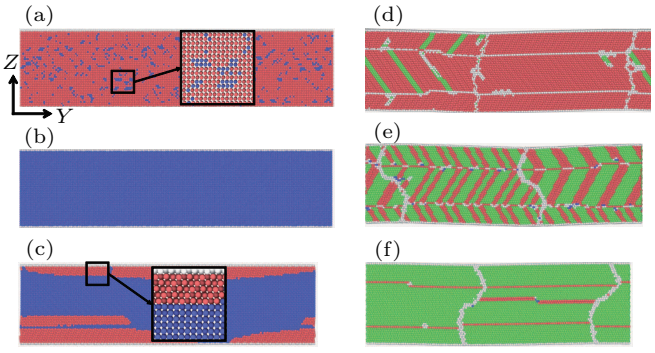

Fig. 6. The atomic configurations of the nanocrystal Ti at different strains when the compression loading is normal to prismatic plane I at 10 K for (a) $\varepsilon = 7.4\%$, (b) $\varepsilon = 9.8\%$, (c) $\varepsilon = 11.7\%$, (d) $\varepsilon = 15.1\%$, (e) $\varepsilon = 20.3\%$, and (f) $\varepsilon = 24.3\%$.

3.3. Plastic deformation of Ti under loading perpendicular to prismatic plane II

3.3.1. Tension loading

The deformation behavior of nanocrystal Ti under tension loading perpendicular to prismatic plane II is demonstrated in Fig. 7. It is interesting that the deformation process is similar to the sample under compression loading normal to prismatic plane I. There are twice phase transformations during the tensile process: the HCP-Ti transforms to BCC-Ti at the strain of 9.2% and then BCC-Ti transforms to HCP-Ti at the strain of 16.9%, as shown in Figs. 7(a)–7(c). At the strain of 17.8%, the BCC-Ti has completely transformed to HCP-Ti. Similar to Fig. 6, there are also some grain boundaries in the newly formed structure, which exhibits the polycrystalline trend during the stretch process. With the increase of tension strain, some SFs occur in the new grains, which arrange symmetrically on both sides of the interfaces, as shown in Fig. 7(e). Figure 7(f) indicates that when the SFs accumulates, FCC-Ti phase generates, accompanied by the movement of HCP SFs. And the inset in Fig. 7(f) shows the orientation relations between HCP and FCC phases is $\langle\bar{1}210\rangle_{\mathrm{HCP}}||\langle 110\rangle_{\mathrm{FCC}}$.

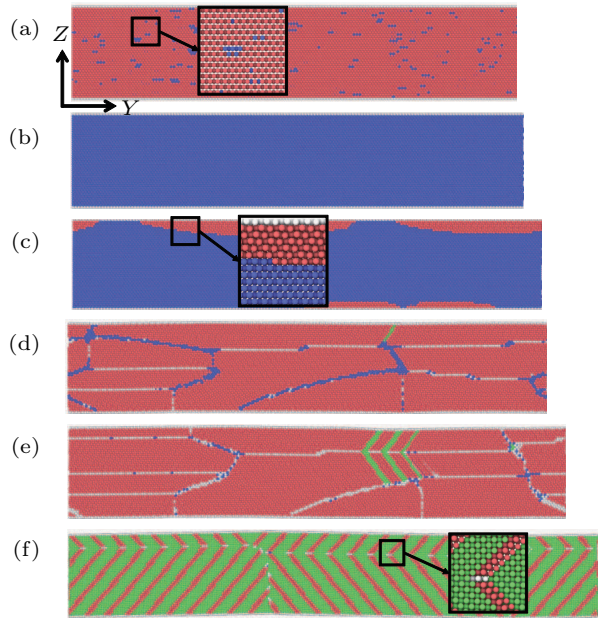

Fig. 7. The atomic configurations of the nanocrystal Ti at different strains when the tension loading is perpendicular to prismatic plane II at 10 K for (a) $\varepsilon = 9.2\%$, (b) $\varepsilon = 9.8\%$, (c) $\varepsilon = 16.9\%$, (d) $\varepsilon = 17.8\%$, (e) $\varepsilon = 21.1\%$, and (f) $\varepsilon = 34.0\%$.

3.3.2. Compression loading

As the compression loading applied perpendicularly to prismatic plane II, the deformation behavior of nanocrystal Ti is particularly given in Fig. 8. The deformation process is similar to the sample, which is normal to prismatic plane I under tension loading at initial stage. It is observed from Fig. 8(a) that some BCC atoms nucleate and generate from both side of the sample at the strain of 8.8%, and the partial enlarged picture describes that the atomic shuffles contributes to the formation of BCC structure. With the increase of compression strain, the plastic deformation behavior of nanocrystal Ti turns to be more complicated. BCC phase grows gradually in laminate, and some BCC structural atoms transform into HCP structure. Meanwhile, dislocations movement and subsequent stacking dislocation growth emerge in the HCP-Ti, as shown in Fig. 8(b). The inset of Fig. 8(b) demonstrates that the orientation of newly formed HCP is different from the original HCP structure. Hereafter, the FCC SFs gradually generate and propagate along the nanocrystal Ti due to the dislocations motion. Meanwhile BCC atoms turn to disappear upon further loading, as shown in Figs. 8(c) and 8(d). And the polycrystalline trend presents during the compression process. As the loading continues, the SFs move constantly in the new grains, which results in the destruction of the free surfaces in both top and bottom of the sample, as shown in Figs. 8(e)–8(f). The enlarged picture in Fig. 8(e) indicates that orientation between HCP structure and FCC SFs is $\{0001\}_{\mathrm{HCP}}||\{111\}_{\mathrm{FCC}}$. It is noted here although there is dense FCC SFs emerging in the nanocrystal Ti, they do not accumulate to form stable FCC phase. Therefore, the plastic deformation of the material at this condition is mainly phase transformation of HCP $\rightarrow$ BCC $\rightarrow$ HCP, which is slightly different from the phenomenon of forming stable FCC phase when tension loading applied vertically to the prismatic plane I.

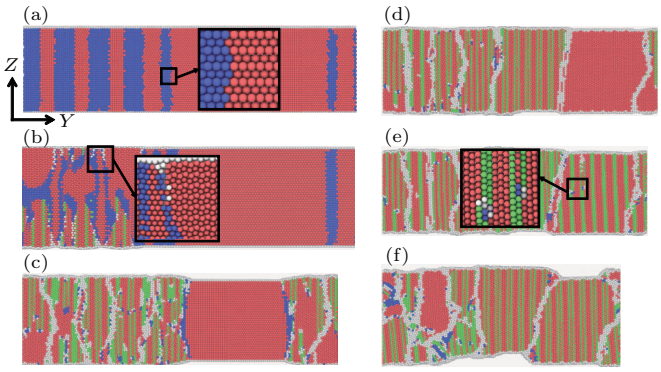

Fig. 8. The atomic configurations of the nanocrystal Ti at different strains when the compression loading is normal to prismatic plane II at 10 K for (a) $\varepsilon = 8.8\%$, (b) $\varepsilon = 9.0\%$, (c) $\varepsilon = 9.5\%$, (d) $\varepsilon = 15.6\%$, (e) $\varepsilon = 17.8\%$, and (f) $\varepsilon = 30.1\%$.

4. Discussion

4.1. Orientation relation for allotropic phase transformation of HCP$\rightarrow$ FCC

As mentioned above, the plastic behaviors of nanocrystal Ti vary with the crystal orientation and loading direction. And the phase transformation has been reported as a representative plastic deformation mechanism in nanocrystal Ti. Especially,

the phase transformation from HCP to FCC lattice has been investigated by numerous researchers. Above these researches, three types of orientation relation (OR) were reported: (I) $\{0001\}_{\rm HCP}||\{111\}_{\rm FCC}$ and $\langle\bar{1}210\rangle_{\rm HCP}||\langle110\rangle_{\rm FCC}$;[20,22,41] (II) $\{10\bar{1}0\}_{\rm HCP}||\{1\bar{1}0\}_{\rm FCC}$ and $\langle0001\rangle_{\rm HCP}||\langle010\rangle_{\rm FCC}$;[15,16,42,43] (III) $\{10\bar{1}0\}_{\rm HCP}||\{111\}_{\rm FCC}$ and $\langle\bar{1}210\rangle_{\rm HCP}||\langle110\rangle_{\rm FCC}$.[20] For the first OR, the interface between two phases is parallel to the basal plane of HCP matrix $\{0001\}$ plane, the OR is denoted as B-type OR. For this type of OR, Zhao *et al.*[22] regarded that the Shockley partial dislocations with Burgers vectors of the $(1/3)\langle10\bar{1}0\rangle$ were generated and glided on (0001) plane during deformed process. Coordinated activation of these partial dislocations gliding on every other (0001) planes gradually converted the HCP structure to the FCC structure. Yu and his coworkers[41] also observed the B-type OR in Ti, and they concluded that the mechanism for HCP-FCC transformation relies on glide of partial dislocations. While for the second OR, the longitudinal boundary between the two phases is parallel to the prismatic plane $(\{10\bar{1}0\}$ plane$)$ of HCP matrix, then the OR is named as P-type OR. However, for the P-type OR, there are some controversy about the mechanism of phase transformation from HCP to FCC phase. Hong *et al.*[42] reported the stress-induced HCP to FCC phase transformation in Ti under cryogenic plane-strain compression, which is in consist with our previous simulation results.[16] Ren[15] simulated the tension properties of Ti nanopillars and found the HCP-FCC transformation, and the P-type OR is caused by the $(1/6)\langle11\bar{2}0\rangle$ Shockley partial dislocations gliding on $\{\bar{1}010\}$ plane. However, Wu *et al.*[43] suggested that either a pure shuffle mechanism or a shear-shuffle mechanism may dominate the deformation mechanism of HCP to FCC transformation for the P-type OR. Zhao and his coworker[22] thought the P-type transformation were attributed to both the pure-shuffle and shear-shuffle mechanisms by successive gliding of opposite-signed 2-layer steps. Furthermore, Yang *et al.*[21] proposed a more detailed mechanism that the FCC phase is preferred after the slip of Shockley partial dislocations of $(1/6)\langle1\bar{2}10\rangle$ on $\{\bar{1}010\}$ planes, and the adjustment of interplanar spacing and the volume expansion were energetically favorable and could happen spontaneously without any energy barrier. The third type of OR is reported by Chen recently.[20] They productively constructed a sandwich model of $\rm HCP_{parent}\rightarrow FCC\rightarrow HCP_{twin}$, in which the orientation between the sandwich structure was $(10\bar{1}0)_{\rm P}||(111)_{\rm FCC}||\{0002\}_{\rm T}$. The double layered $(\bar{1}010)_{\rm P}$ planes of the parent phase were transformed to the (111) planes of the FCC crystal. Concurrently, the $\{0002\}_{\rm T}$ planes of the parent are transformed to the $(11\bar{1})$ planes of the FCC crystal. But the double layered $(\bar{1}010)_{\rm P}$ planes could not transform to the layered $(111)_{\rm FCC}$ planes by shear and atomic shuffles.

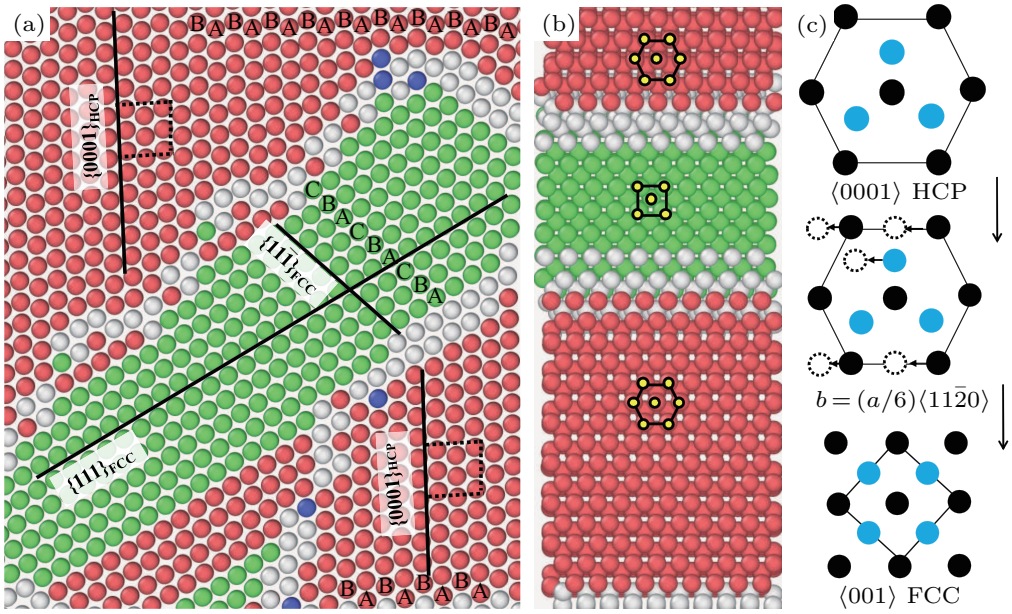

Fig. 9. The close inspections of the transformation from HCP configuration to FCC configuration presented in Fig. 4(b).

In the present work, we have observed both B-type OR and P-type OR during the HCP to FCC phase transformation, and different type of orientation relationships have been listed in Table 1. Further exploring, figure 9 shows the detailed OR of the transformation from HCP to FCC structure in Fig. 4(b). It is observed from Fig. 9 that the OR belongs to the P-type OR. The slip of $(1/6)\langle11\bar{2}0\rangle$ Shockley partial dislocations on $\bar{1}010$ plane is accounted for the phase transformation, which is indicated by Fig. 9(c). According to the dislocations analysis, the $\boldsymbol{c}+\boldsymbol{a}$ dislocations with Burgers vector of $\boldsymbol{b}=(1/3)\langle\bar{1}\bar{1}23\rangle$

have also been activated during the deformation, which glide on $\{\bar{1}101\}$ planes continuously. This OR has been detailedly reported in our previous work,[16,44] and the transformation process is found to be induced by the local stress concentration.

While for the B-type OR, figure 10 presents the enlarged drawing of the HCP to FCC phase transformation of Fig. 6(e). The B-type OR is observed with the OR of $\{0001\}_{\rm HCP}||\{111\}_{\rm FCC}$ and $\langle\bar{1}210\rangle_{\rm HCP}||\langle 110\rangle_{\rm FCC}$, as shown in Fig. 10(a). The DXA indicates that the Shockley partial dislocations with Burgers vectors of the $(1/3)\langle 10\bar{1}0\rangle$ generate and glide on (0001) plane during the compression process, which is the underlying plastic mechanism for the transformation of HCP to FCC phase. Furthermore, there are deformation twins (white lines represent twins in FCC structure, and black lines represent twins in HCP structure, as shown in Fig. 10(a)) at the internal grains, which also owes to the dislocations glide on the certain crystallographic planes. Dislocations propagation promotes the phase transformation of HCP to FCC structure, and simultaneously activates twinning deformation at different crystal structures. Therefore, the nanocrystalline Ti possesses better plastic properties under the compression loading applied along $[10\bar{1}0]$ axis.

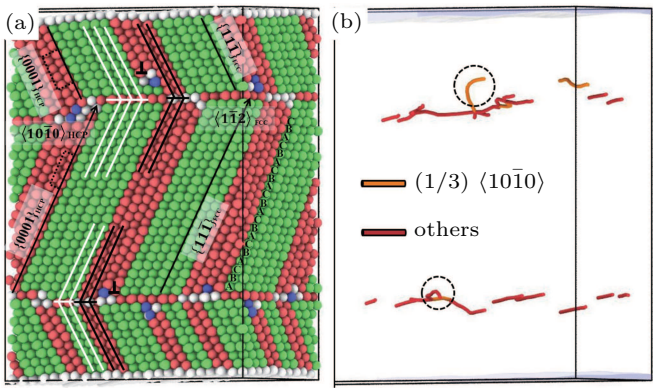

Fig. 10. The partial enlarged drawing of the HCP to FCC phase transformation shown in Fig. 6(e).

4.2. Mechanism for allotropic phase transformation of HCP→ BCC→ HCP

It is observed from Figs. 6–8 that there is a phase transformation from HCP to BCC, and BCC phase transforms to HCP phase again. Searching for more details of the phase transformation of HCP → BCC → HCP, the microstructure evolution of nanocrystal Ti under compression loading is taken as an example. Figure 11 shows the OR of HCP and BCC during the transformation. It should be mentioned that the HCP phase has transformed to BCC completely at a certain critical strain. For simplicity, the HCP phase before the critical strain is defined as α_1-Ti, and BCC phase is defined as β-Ti, while the HCP phase after the critical strain is defined as α_2-Ti. In the process of transformation of HCP to BCC phase, the atoms in the basal plane of HCP structure are shuffled from the initial 60° to 70.53° between the two adjacent $\langle 11\bar{2}0\rangle$ directions. The HCP structure is deformed to be a narrow hexagon, in which the atoms in A layer is stretched, while the atoms in B layer move to the center of the rhombus formed by movement of the atoms in A layer. Then the BCC structure generates and the orientation relationship between the α_1-Ti and the β-Ti is $\{0001\}_{\alpha1}||\{110\}_{\beta}$ and $\langle 11\bar{2}0\rangle_{\alpha1}||\langle 11\bar{1}\rangle_{\beta}$, as shown in Fig. 11(a). Analogously, repeating shuffle sequence of group of atoms on every $\{110\}$ BCC plane by the same shuffling magnitude finally forms the HCP nucleus, which results in the OR of between the β-Ti and α_2-Ti is $\{110\}_{\beta}||\{0001\}_{\alpha2}$ and $\langle 11\bar{1}\rangle_{\beta}||\langle 11\bar{2}0\rangle_{\alpha2}$, as shown in Fig. 11(b). One thing is noted here is that the view direction of Fig. 11(b) is along $\langle 10\bar{1}0\rangle_{\alpha1}$ direction. That is to say, the allotropic phase HCP → BCC → HCP of the nanocrystal Ti during the compression loading has an OR of $\{0001\}_{\alpha1}||\{110\}_{\beta}||\{10\bar{1}0\}_{\alpha2}$. Summarily, atomic shuffles are needed both in the processes of HCP-BCC transformation and BCC-HCP transformation. The results in present work consist with the conclusion in Ref. [1].

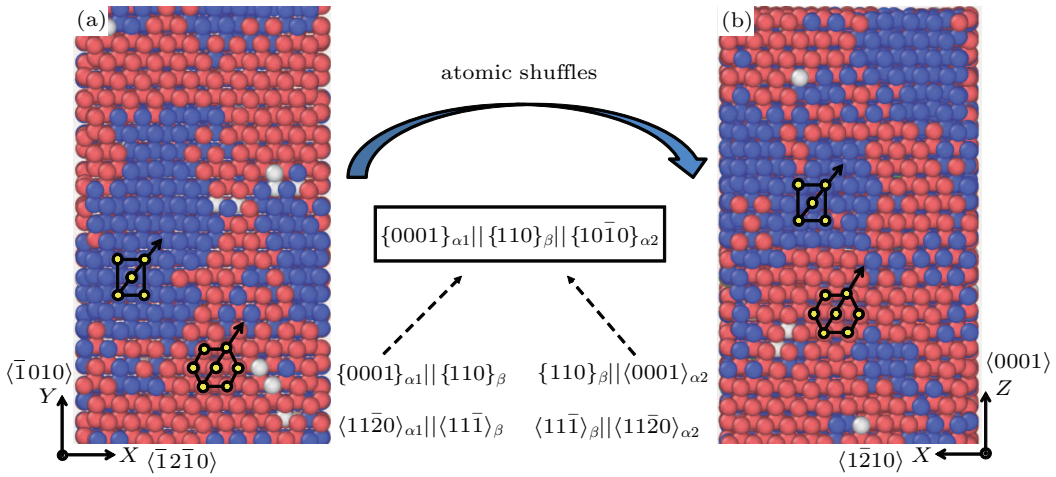

Fig. 11. The transformation from (a) HCP to BCC at compressive strain of 6.8% and (b) BCC to HCP at compressive strain of 8.7%.

Table 1. Main plastic deformation behaviors of nanocrystal Ti under different loading directions.

Model	Loading direction	Main plastic deformation behaviors	Orientation relationship of FCC phase transformation
Basal plane	Tension	Grain reorientation → deformation twinning	–
	Compression	Phase transformation: HCP → FCC	P-type
Prismatic plane I	Tension	Phase transformation: HCP → BCC → FCC	P-type
	Compression	Phase transformation: HCP → BCC → HCP → FCC	B-type
Prismatic plane II	Tension	Phase transformation: HCP → BCC → HCP → FCC	B-type
	Compression	Phase transformation: HCP → BCC → HCP (with dense FCC SFs)	B-type

Table 1 summarizes the main plastic behavior of nanocrystalline Ti at different crystal orientations and loading directions. As the table indicated, the plasticity of nanocrystalline Ti not only shows tension–compression asymmetry, but also exhibits crystal lattice orientation anisotropy. Compared with BCC and FCC crystals, the slip system of HCP crystal is relatively limited. Thence, the plastic deformation behavior is mainly dominated by grain reorientation, phase transformation or other forms, while dislocations motion is relatively difficult to activate. Furthermore, due to lower spatial symmetry than the two crystal structures mentioned previously (FCC and BCC), the deformation behavior of nanocrystalline Ti actually shows anisotropic plasticity.

4.3. Energy evolution of phase transformation during loading process

Actually, energy evolution of nanocrystal Ti under various loading process also shows anisotropic plasticity. Different plastic deformation mechanisms in loading process indicate the different energy evolution paths. Therefore, the energy evolution in the loading process should be paid more attention to, especially in the case of different phase transformation mechanisms. Figure 12 expounds the potential energy evolution during the loading process. For simplicity without loss of generality, only two cases of tension loading, *i.e.*, $[\bar{1}010]$ tension and $[\bar{1}2\bar{1}0]$ tension models are plotted in Fig. 12, and the red stars indicate inflection points of the energy–strain curves. Meanwhile, the atomic fraction-strain curves of HCP, FCC, and BCC structures have also been plotted to obtain a more intuitive transformation process. Obviously, the energy evolution present different trends when tension loading is applied along the $[\bar{1}010]$ and $[\bar{1}2\bar{1}0]$ axes. For the case of $[\bar{1}010]$ tension, a phase transformation of HCP → BCC → FCC is presented in Fig. 12(a), and a transient BCC phase transformation is observed. As is shown in Fig. 12(a) that the HCP has the lowest potential energy (−4.842 eV/atom) at the equilibrium lattice parameter (0.295 nm). There is high potential energy barriers of 53 meV/atom needed to be overcome when the HCP-Ti transforms to BCC-Ti. While the energy difference between HCP and FCC structures is 16 meV/atom when the FCC begins to occur. While for the case of $[\bar{1}2\bar{1}0]$ tension, more complicated phase transition of HCP → BCC → HCP → FCC and a stable BCC phase transformation are shown in Fig. 12(b). It is observed that a potential energy barriers of 21 meV/atom needed to be overcome when the HCP-Ti transforms to BCC-Ti, and the BCC-Ti is a stable state. While the BCC-Ti have to overcome the potential energy barriers of 3 meV/atom when it transforms to HCP-Ti. When the FCC-Ti structure begins to generate, the potential energy is 11 meV/atom lower than the initial HCP-Ti, which is lower than the case of $[\bar{1}010]$ tension. That is to say, on one hand, the energy of the multi-stage transformation of HCP → FCC is more stable, which is more favorable to maintain plastic deformation; on the other hand, the phase transformation is an energy triggered process. Chen *et al.*[20] reported that the energy in HCP is 30 meV/atom lower than that of the BCC, and 10 meV/atom lower than that of the FCC when a monocrystal Ti is taken into consideration (*i.e.*, just one state HCP, FCC or BCC exist). The result is obviously different from the results of this work, the reason is attributed to that there are three states of HCP, BCC, and FCC concomitant during this process, and the grain boundary, the SFs boundary and twin boundary exist in the sample.

The energy evolution of nanocrystal Ti under compression loading applied for the prismatic plane is the same trends as the tension case. The difference is that the compression along the $[\bar{1}010]$ axis is more complicated, and the energy barrier is smaller. In addition, the phase transition (HCP → FCC) with compression loading applied along the *c* axis also has a high energy barrier. Above all, these do indicate anisotropic plasticity during deformation of nanocrystal Ti. What should be emphasized here is that the potential energy of the system is only related to the relative positions of the neighboring atoms. Combining with the energy evolution and microstruc-

ture evolution under different loading conditions, the plastic anisotropy is mainly related to the arrangement of atoms. Different lattice planes have different atomic stacking forms, and atoms move in different paths when loading is applied, which finally leads to the anisotropic plasticity. In the present work, we only selected a few special lattice planes, and obtained the anisotropic plasticity of nanocrystal Ti during different loading processes. Actually, there are many other crystal planes and forms of loading, much more attention should be paid to obtain in-depth mechanisms of anisotropic plasticity of nanocrystal Ti.

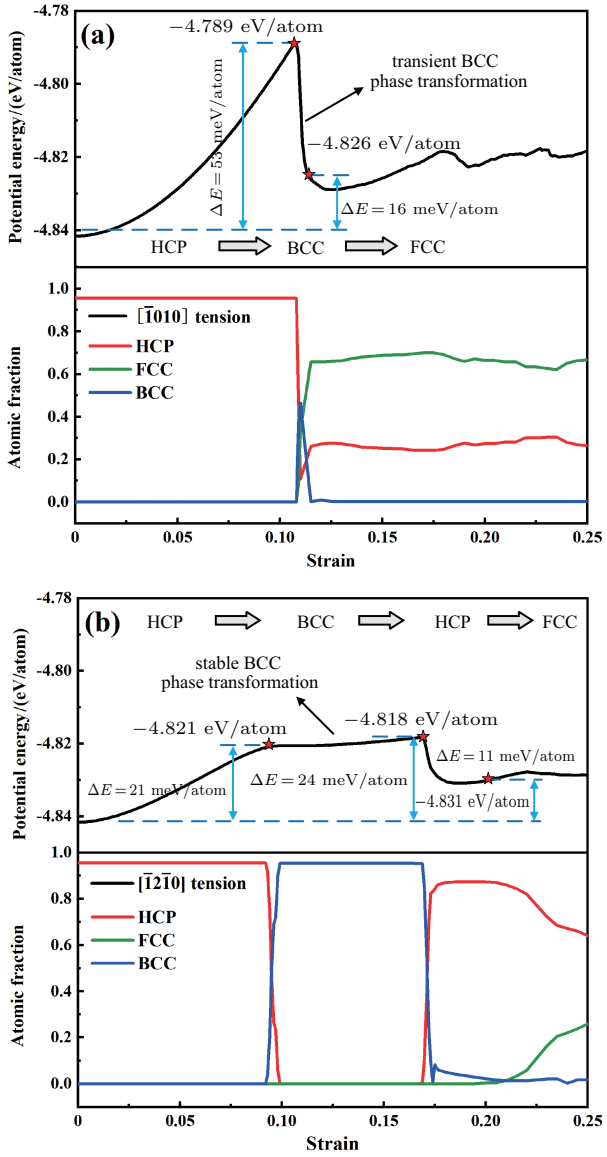

Fig. 12. The potential energy evolution of phase transformation during the tension process. (a) $[\bar{1}010]$ tension and (b) $[\bar{1}2\bar{1}0]$ tension.

5. Conclusions

We have performed MD simulations to study the effect of crystal orientation and loading condition on the mechanical properties of nanocrystal Ti. The results show that the deformation behavior under different crystal orientations and loading directions presents anisotropic plasticity. The conclusions of this paper are as follows:

(I) Under loading vertical to basal plane, the deformation mechanisms change with the loading direction. In case of the tension process, the deformation mechanism is the formation of "new grains" and subsequent deformation twinning. For the compression process, the transformation from HCP to FCC phase dominates the plastic deformation, which is due to the numerous dislocations propagation and accumulation of dense SFs.

(II) Under tension loading vertical to prismatic plane I, the deformation mechanism is phase transformation of HCP → BCC → FCC. Atomic shuffles of the partial basal atoms accounts for the phase transition of HCP → BCC phase, while FCC phase is induced by the glide dislocations and movement of stacking faults. While under compressive load, the phase transformation of HCP → BCC → HCP → FCC is observed, as well the subsequent movement of SFs in FCC crystal.

(III) Under tension loading vertical to prismatic plane II, the deformation mechanism is mainly manipulated by the phase transformation of HCP → BCC → HCP → FCC. For the compression case, the phase transformation from HCP → BCC → HCP dominates the plastic deformation.

(IV) During the deformation, both the B-type orientation relationship of $\{0001\}_{\mathrm{HCP}}||\{111\}_{\mathrm{FCC}}$ and $\langle\bar{1}210\rangle_{\mathrm{HCP}}||\langle 110\rangle_{\mathrm{FCC}}$, and P-type orientation relationship of $\{10\bar{1}0\}_{\mathrm{HCP}}||\{1\bar{1}0\}_{\mathrm{FCC}}$ and $\langle 0001\rangle_{\mathrm{HCP}}||\langle 010\rangle_{\mathrm{FCC}}$ are observed between the HCP and FCC phases. Meanwhile, the orientation relationship between the HCP and BCC phases are $\{0001\}_{\alpha 1}||\{110\}_{\beta}||\{10\bar{1}0\}_{\alpha 2}$, during the process of transformation of HCP → BCC → HCP.

(V) Energy evolution also shows anisotropic plasticity, and multistage phase transformation is more stable, which is more favorable to maintain plastic deformation. The plastic anisotropy of nanocrystalline Ti is determined by the stacking order of the atoms.

References

[1] Leyens C and Peters M 2003 *Titanium and Titanium Alloys: Fundamentals and Applications* (Darmstadt: Wiley-VCH) pp. 25–35

[2] Zhang Y F, Xue S, Li Q, Li J, Ding J, Niu T J, Su R, Wang H and Zhang X 2019 *Acta Mater.* **175** 466

[3] Elias C N, Lima J H C, Valiev R, *et al.* 2008 *Jom* **60** 46

[4] Das J, Kim K B, Baier F, Löser W and Eckert J 2005 *Appl. Phys. Lett.* **87** 161907

[5] Peters M, Kumpfert J, Ward C H and Leyens C 2003 *Adv. Eng. Mater.* **5** 419

[6] Banerjee D and Williams J C 2013 *Acta Mater.* **61** 844

[7] Xiao L 2005 *Mater. Sci. Eng. A* **394** 168

[8] Wang Q, Yin Y, Sun Q, Xiao L and Sun J 2014 *J. Mater. Res.* **29** 569

[9] Liu B Y, Wang J, Li B, Lu L, Zhang X Y, Shan Z W, Li J, Jia C, Sun J and Ma E 2014 *Nat. Commun.* **5** 3297

[10] Liu B Y, Wan L, Wang J, Ma E and Shan Z W 2015 *Scr. Mater.* **100** 86

[11] Wang J, Liu L, Tomé C N, Mao S X and Gong S K 2013 *Mater. Res. Lett.* **1** 81

[12] Tu J and Zhang S 2016 *Mater.* **96** 143
[13] Ni C, Ding H and Jin X 2016 *Comput. Mater. Sci.* **111** 163
[14] Chen P, Wang F and Li B 2019 *Comput. Mater. Sci.* **164** 186
[15] Ren J, Sun Q, Xiao L, Ding X and Sun J 2014 *Comput. Mater. Sci.* **92** 8
[16] An M, Deng Q, Li Y, Song H, Su M and Cai J 2017 *Mater.* **127** 204
[17] Yu Q, Sun J, Morris J W Jr and Minor A M 2013 *Scr. Mater.* **69** 57
[18] Ren J, Sun Q, Xiao L, Ding X and Sun J 2014 *Mater. Sci. Eng. A* **615** 22
[19] Yu Q, Li S, Minor A M, Sun J and Ma E 2012 *Appl. Phys. Lett.* **100** 063109
[20] Chen P, Wang F and Li B 2019 *Acta Mater.* **171** 65
[21] Yang J X, Zhao H L, Gong H R, Song M and Ren Q Q 2018 *Sci. Rep.* **8** 1992
[22] Zhao H, Hu X, Song M and Ni S 2017 *Scr. Mater.* **132** 63
[23] An M, Song H and Su J 2012 *Chin. Phys. B* **21** 106202
[24] Shahzad A, He M, Ghani S, Kashif M, Munir T and Yang F 2019 *Chin. Phys. B* **28** 055201
[25] Li Y, Cai J, Mo D and Wang Y 2018 *Chin. Phys. B* **27** 086401
[26] Liu Q, Guo Q N, Qian X F, Wang H N, Guo R L, Xiao Z J and Pei H J 2019 *Acta Phys. Sin.* **68** 133101 (in Chinese)
[27] Li Y and Peng P 2019 *Acta Phys. Sin.* **68** 076401 (in Chinese)
[28] Li R, Liu T, Chen X, Chen S C, Fu Y H and Liu L 2018 *Acta Phys. Sin.* **67** 190202 (in Chinese)
[29] Lee B J 2007 *Calphad* **31** 95
[30] Lee B J and Baskes M 2000 *Phys. Rev. B* **62** 8564
[31] Wang X H, Shen W H, Huang X F, Zang J L and Zhao Y P 2017 *Sci. China-Phys. Mech. Astron.* **60** 064612
[32] Wadley H N G, Zhou X, Johnson R A and Mechanisms M 2001 *Progr. Mater. Sci.* **46** 329
[33] Zhou X W, Wadley H N G, Johnson R A, Larson D J, Tabat N, Cerezo A, Petford-Long A K, Smith G D W, Clifton P H, Martens R L and Kelly T F 2001 *Acta Mater.* **49** 4005
[34] Wan L, Yu X X, Zhou X and Thompson G 2016 *J. Appl. Phys.* **119** 245302
[35] Su M J, Deng Q, An M R, Liu L T and Ma C B 2019 *Comput. Mater. Sci.* **158** 149
[36] Rao S I, Akdim B, Antillon E, Woodward C, Parthasarathy T A and Senkov O N 2019 *Acta Mater.* **168** 222
[37] Faken D and Jónsson H 1994 *Comput. Mater. Sci.* **2** 279
[38] Stukowski A 2010 *Modell. Simul. Mater. Sci. Eng.* **18** 015012
[39] Li D, Wang F C, Yang Z Y and Zhao Y P 2014 *Sci. China-Phys. Mech. Astron.* **57** 2177
[40] Stukowski A, Bulatov V V and Arsenlis A 2012 *Model. Simul. Mater. Sci. Eng.* **20** 085007
[41] Yu Q, Kacher J, Gammer C, Traylor R, Samanta A, Yang Z and Minor A M 2017 *Scr. Mater.* **140** 9
[42] Hong D H, Lee T W, Lim S H, Kim W Y and Hwang S K 2013 *Scr. Mater.* **69** 405
[43] Wu H C, Kumar A, Wang J, Bi X F, Tomé C N, Zhang Z and Mao S X 2016 *Sci. Rep.* **6** 24370
[44] An M R, Deng Q, Su M J, Song H Y and Li Y L 2017 *Mater. Sci. Eng. A* **684** 491